FULL PAPER

High-Performance All-Polymer Photoresponse Devices Based on Acceptor–Acceptor Conjugated Polymers

Xiaofen Wang, Lei Lv, Lingliang Li, Yusheng Chen, Kai Zhang, Haoran Chen, Huanli Dong, Jinsong Huang, Guozhen Shen,* Zhou Yang,* and Hui Huang**

Three acceptor–acceptor (A–A) type conjugated polymers based on isoindigo and naphthalene diimide/perylene diimide are designed and synthesized to study the effects of building blocks and alkyl chains on the polymer properties and performance of all-polymer photoresponse devices. Variation of the building blocks and alkyl chains can influence the thermal, optical, and electrochemical properties of the polymers, as indicated by thermogravimetric analysis, differential scanning calorimetry, UV–vis, cyclic voltammetry, and density functional theory calculations. Based on the A–A type conjugated polymers, the most efficient all-polymer photovoltaic cells are achieved with an efficiency of 2.68%, and the first all-polymer photodetectors are constructed with high responsivity (0.12 A W^{-1}) and detectivity (1.2×10^{12} Jones), comparable to those of the best fullerene based organic photodetectors and inorganic photodetectors. Photoluminescence spectra, charge transport properties, and morphology of blend films are investigated to elucidate the influence of polymeric structures on device performances. This contribution demonstrates a strategy of systematically tuning the polymeric structures to achieve high performance all-polymer photoresponse devices.

1. Introduction

In the past decades, conjugated polymers have been employed as active materials for organic electronics, including photovoltaics[1] and photodetectors (PDs).[2] In comparison to their inorganic counterparts, conjugated polymers possess several advantages.[3] Their solution processibility enables the potentially simple and low cost fabrication. Furthermore, conjugated polymers can offer light weight and mechanic flexibility and tunable optoelectronic properties through structure engineering. In order to achieve low dark current and high external quantum efficiency (EQE), bulk heterojunction structure with a blend of donors and acceptors as active materials has been used to construct organic photovoltaics (OPVs)[4] and PDs.[2a,5] In comparison to the various conjugated polymers for donors, the fullerene derivatives are dominant for electron acceptors due to their high electron mobility and fast split of excitons.[6] However, the fullerene derivatives are not the optimal acceptors due to their relatively high cost and intrinsically low extinction coefficient in visible region.[7]

Recently, n-type conjugated polymers have been used to construct complementary metal oxide semiconductors (CMOS)[8] and all-polymer solar cells[3,8a,9] as alternative for fullerene due to their merits of the potentially low-cost synthesis and tunable and strong absorption for light. Through materials and device engineering, now the highest efficiency for all-polymer solar cells is over 7%.[9a] Among them, naphthalene diimide (NDI) and perylene

X. Wang, L. Lv, Y. Chen, Prof. H. Huang
College of Materials Science and Opto-Electronic Technology and Key Laboratory of Vacuum Physics
University of Chinese Academy of Sciences
Beijing 100049, P. R. China
E-mail: huihuang@ucas.ac.cn

X. Wang, Prof. Z. Yang
Beijing Key Laboratory of Function Materials for Molecular & Structure Construction
School of Materials Science and Engineering
University of Science and Technology Beijing
Beijing 100083, P. R. China
E-mail: yangz@ustb.edu.cn

L. Li, Prof. J. Huang
Department of Mechanical and Materials Engineering
Nebraska Center for Materials and Nanoscience
University of Nebraska
Lincoln, NE 68588-0656, USA
E-mail: jhuang2@unl.edu

K. Zhang, H. Chen, Prof. G. Shen
State Key Laboratory for Superlattices and Microstructures
Institute of Semiconductors
Chinese Academy of Sciences
Beijing 100083, China
E-mail: gzshen@semi.ac.cn

Dr. H. Dong
Beijing National Laboratory for Molecular Sciences
Key Laboratory of Organic Solids
Institute of Chemistry
Chinese Academy of Sciences
Beijing 100190, China

DOI: 10.1002/adfm.201601745

diimide (PDI) based n-type conjugated polymers constructed by donor–acceptor (D–A) strategy are an important class.[8] NDI and PDI-based conjugated polymers were observed to exhibit high electron transport, which may be attributed to their fused and planar structures with strong electron deficient characteristics.[10] For example, Gao et al. employed NDI-bithophene polymer as an acceptor to achieve efficiency as high as 8.27%.[9q] On the other side, acceptor–acceptor (A–A) strategy is another method to achieve air-stable n-type conjugated polymers for organic electronics.[9m,11] Zhan and co-workers employed PDI and fluorenone units to synthesize A–A copolymers with good air stability.[11c] Ober and co-workers reported A–A copolymers based on 2-alkylbenzotriaole and 2,1,3-benzothiadiazole (BT) for organic field effect transistors (OFET) (μ_e = 0.01 cm^2 V^{-1} s^{-1})[11a] and all-polymer solar cells (η = 0.31%).[11b] Later, benzotriazole unit was employed to copolymerize with other electron-deficient units, such as quinoxaline and benzobisthiadiazole, to achieve A–A copolymers for all-polymer solar cells as acceptors with an efficiency of 0.40%.[11e] Reynolds and co-workers also synthesized A–A copolymers based on isoindigo and BT and employed them for electron acceptor for all-polymer solar cells with the best efficiency of 0.47%.[9m] Recently, two A–A copolymers based on PDI and BT were synthesized and employed for all polymer solar cells to achieve an efficiency of 0.31%.[11d] Very recently, a couple of A–A conjugated polymers with B←N building blocks were synthesized and employed as acceptors for high performance all-polymer solar cells by Liu and co-workers.[12] Obviously, A–A copolymers have rarely been employed as electron acceptors for high-efficiency all-polymer solar cells, even though they exhibit excellent electron transport mobility and air stability.

Here, we report three novel NDI and PDI-based n-type conjugated polymers constructed by A–A strategy. Tuning structures of the polymers through changing building blocks and alkyl chains, we achieved high performance all-polymer photovoltaics and PDs. The PTB7-Th:PIIG-PDI(2-octyldodecyl (OD)) based solar cells afford a maximum efficiency of 2.68%, which is one of the highest efficiencies for solar cells with A–A polymers as acceptors. For all-polymer PDs, the responsivity is 0.12 A W^{-1} and the detectivity reaches 10^{12} Jones, among those of the fullerene based organic[2j] and inorganic PDs.[13] To the best of our knowledge, this is the first high performance all-polymer broadband organic photodetectors (OPD). Furthermore, the optical absorption, photoluminescence, charge transport, and morphology of blend films were investigated to probe the performances of all-polymer photoresponse devices.

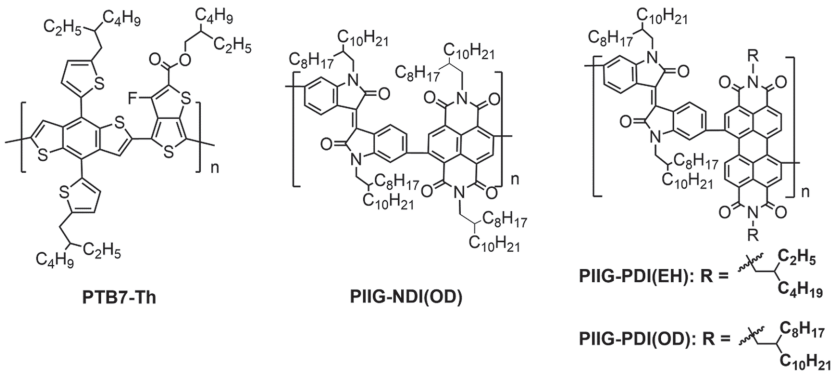

Figure 1. Chemical structures of PTB7-Th, PIIG-NDI(OD), PIIG-PDI(EH), and PIIG-PDI(OD).

2. Results and Discussion

2.1. Synthesis and Characterization of N-Type Polymers

Three n-type conjugated polymers PIIG-NDI(OD), PIIG-PDI(2-ethylhexyl (EH)), and PIIG-PDI(OD) (**Figure 1**) were synthesized through Suzuki coupling of diborate-isoindigo (IIG) and dibromo-NDI or dibromo-PDI in 60%–70% yields as shown in Scheme S1 (Supporting Information). The physicochemical properties of polymers were summarized in **Table 1**. The molecular weights (M_w) of PIIG-NDI(OD), PIIG-PDI(EH), and PIIG-PDI(OD) by gel permeation chromatography (GPC) are 32.6 KDa (*Polydispersity index, PDI* = 2.01), 71.2 KDa (*PDI* = 2.64), and 64.6 KDa (*PDI* = 2.34). These polymers were fully characterized by ^{1}H NMR spectroscopy (broad features as expected, Figures S1–S3, Supporting Information), thermogravimetric analysis (TGA), differential scanning calorimetry (DSC), optical spectroscopy, electrochemistry, and elemental analysis (see the Experimental Section for details).

2.2. Thermal Properties

TGA (heating ramp rate = 10 °C min^{-1} under N_2) was used to investigate polymer thermal properties (Figure S4, Supporting Information), with a 5% mass loss defined as the thermolysis threshold. The thermolysis onset temperatures for all polymers are higher than 400 °C, indicative of excellent thermal stability. The thermal properties of the new polymers were also examined by DSC (Figure S5, Supporting Information). PIIG-NDI(OD) demonstrated a single endothermic peak at 257 °C, which is tentatively attributed to backbone melting, and an exothermic recrystallization peak upon cooling at 251 °C. However, both PIIG-PDI(EH) and PIIG-PDI(OD) showed no detectable endothermic or exothermic peaks, indicative of amorphous characteristics.

2.3. Optical Absorption Properties and Density Functional Theory (DFT) Calculations

Figure 2 shows the solution and thin-film optical absorption spectra of polymers and blend films of PTB7-Th:polymer, and data are collected in Table 1. Due to the presence of multiple transitions, solid state optical band gaps (E_g) were estimated from the low-energy band edges in the spectra.[14]

In the 1,2-dichlorobenzene (DCB) solution, all three copolymers exhibit two strong absorption bands in the range of 350–500 nm and 500–700 nm. The absorption spectrum of PIIG-NDI(OD) exhibits fine structures with three peaks in the

Table 1. Summary of thermal, optical absorption, and electrochemical properties of polymers PIIG-NDI(OD), PIIG-PDI(EH), and PIIG-PDI(OD).

Polymers	$E_g^{optical}$ [a)] [eV]	$E^{red-1/2}$ [V]	LUMO [b)] [eV]	HOMO [c)] [eV]	T_{TGA} [°C]	$\lambda_{max}^{solution}$ [nm]	$\lambda_{max}^{thin-film}$ [nm]
PIIG-NDI(OD)	1.75	−0.51	−3.93	−5.68	420	365, 384, 421, 553	369, 387, 426, 599
PIIG-PDI(EH)	1.72	−0.42	−4.02	−5.74	431	430, 542	430, 523
PIIG-PDI(OD)	1.70	−0.45	−3.99	−5.69	444	431, 541	430, 529

[a)]Calculated from equation: $E_g = 1240/\lambda$, λ is the low energy band edge wavelength of optical spectra; [b)]Estimated from equation: $E_{LUMO} = -4.44$ eV $- E^{red\text{-}1/2}$; [c)]Calculated from: $E_{HOMO} = E_{LUMO} - E_g$.

short wavelength range, indicating a relatively rigid backbone, while PIIG-PDI(EH) and PIIG-PDI(OD) exhibit broad peaks in both two bands. The shorter wavelength feature was tentatively ascribed to a π–π^* transition of the NDI or PDI building block, while the lower energy band is tentatively assigned to a one-electron highest occupied molecular orbital (HOMO) → lowest unoccupied molecular orbital (LUMO) excitation, similar to the reported A–A conjugated polymers.[11d] As intramolecular charge transfer (ICT) bands are often observed in D–A conjugated polymers, it is rare to be observed in A–A conjugated polymers. The study of origination of the bands is under investigation. The absorption maxima of PIIG-PDI(EH) (430, 542 nm) and PIIG-PDI(OD) (431, 541 nm) are intrinsically same, showing that the different alkyl chains have negligible influence on their UV–vis absorption properties.

In thin films, the absorption maxima of PIIG-NDI(OD) (369, 387, 426, 599 nm) showed small red shifts in short wavelength range and moderate red shift in long wavelength range in comparison to those of the solution state, suggesting moderate aggregation in the solid state. The absorption maxima of PIIG-PDI(EH) and PIIG-PDI(OD) are 430 and 523 nm, and 430 and 529 nm, respectively. In comparison to the solution state, the absorption maxima of both PIIG-PDI polymers in the short wavelength range are similar, while those in long wavelength range showed a small blue shift, indicating little aggregation in the solid state. This is consistent with the DSC results that PIIG-NDI(OD) exhibits melting and recrystallization peaks, while two PIIG-PDI polymers demonstrated amorphous characteristics. Furthermore, the extinction coefficients of thin films are shown in Figure S6 (Supporting Information), which demonstrated that the extinction coefficients of PIIG-PDI(EH), and PIIG-PDI(OD) are higher than that of PIIG-NDI(OD) in the range of 450–700 nm. This is consistent with the photocurrents of photoresponse devices as discussed in the next part. From the low-edge onsets of absorption, the optical bandgaps of PIIG-NDI(OD), PIIG-PDI(EH), and PIIG-PDI(OD) were estimated to be 1.75, 1.72, and 1.70 eV, respectively, similar to other NDI or PDI-based A–A conjugated polymers.[11c]

As shown in Figure 2c, the UV–vis absorptions of PTB7-Th:acceptors blend films have a broad coverage from 300 to 780 nm, showing that the blend films may be excellent light absorbers. Furthermore, both PTB7-Th:PIIG-PDI(EH) and PTB7-Th:PIIG-PDI(OD) demonstrated a more intense absorption than PTB7-Th:PIIG-NDI(OD) in the range of 350–600 nm, which suggests the former systems may absorb more light to generate higher short-circuit currents (J_{SC}).

Structurally, PIIG-NDI and PIIG-PDI polymers differ from each other based on the identity of accepting building blocks (NDI and PDI) conjugated with IIG unit. The difference in absorption spectra can be attributed to two parameters: the electron accepting capability of the moieties (NDI and PDI) neighboring IIG along the backbone and the dihedral angle between the IIG unit and its neighboring units (NDI and PDI). On the basis of these considerations, time-dependent DFT (TDDFT)[15] calculations at the B3LYP/6-31G** level were also performed on the polymer building blocks to provide insights into the electronic structure of the corresponding copolymers. As shown in **Figure 3**a, the optimized geometries of IIG-NDI and IIG-PDI systems demonstrated that the dihedral angle between IIG and NDI is ≈62°, similar to that between IIG and PDI (61°), while PDI itself also adopts a twisted angle of 11°. This indicates that PIIG-NDI may form moderate aggregation in the solid state while PIIG-PDI adopts little aggregation, accordant with their UV–vis characteristics. Figure 3b showed the frontier orbital density distributions for IIG-NDI and IIG-PDI. In IIG-NDI, the HOMO is dominated by IIG unit while

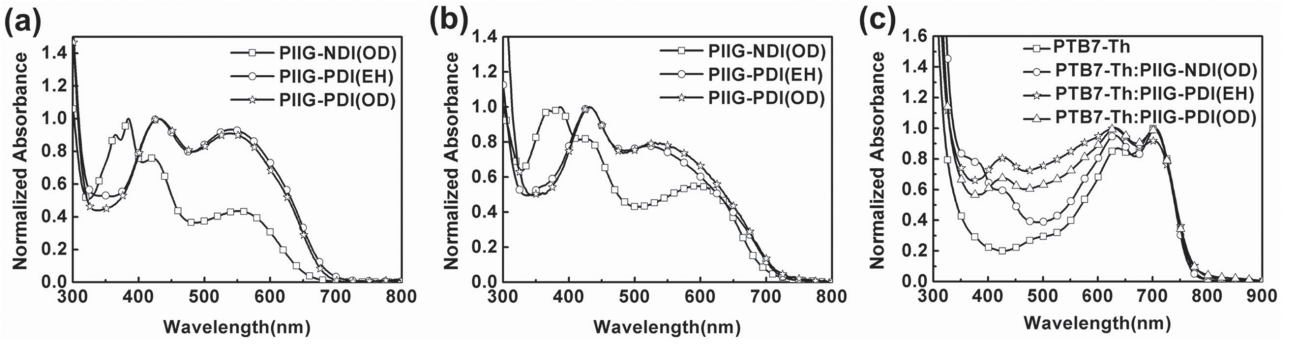

Figure 2. a) Optical absorption spectra of polymers PIIG-NDI(OD), PIIG-PDI(EH), and PIIG-PDI(OD) in DCB solution; b) as-cast pristine films on glass substrates; c) blend films with PTB7-Th on glass substrate.

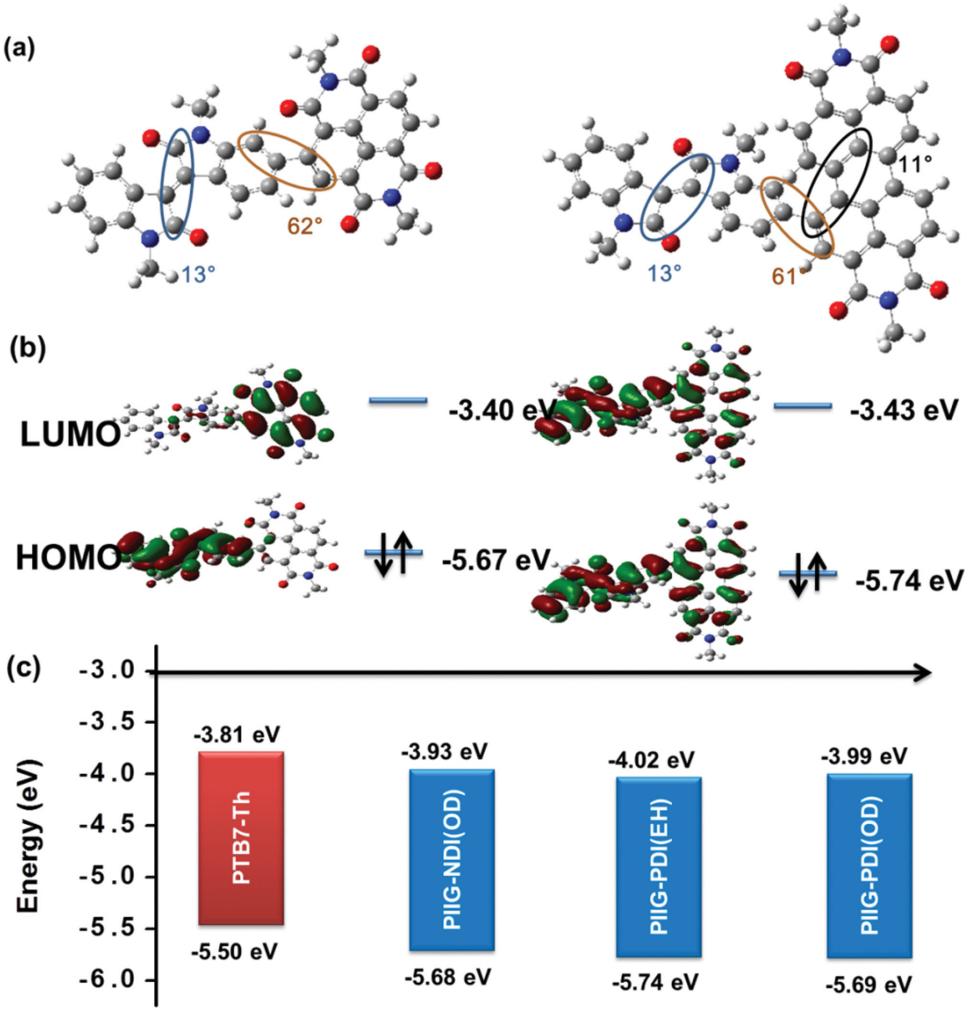

Figure 3. a) The optimized geometries of IIG-NDI and IIG-PDI systems based on computation on DFT//B3LYP/6-31G** level, and b) the frontier orbital density distributions for IIG-NDI and IIG-PDI, and c) experimentally determined energy levels of PTB7-Th, PIIG-NDI(OD), PIIG-PDI(EH), and PIIG-PDI(OD).

the LUMO is localized on the NDI, which supports the existence of the ICT in the A–A copolymer. However, the HOMO and LUMO are distributed on both IIG and PDI building blocks, which indicates that IIG and PDI have similar electron accepting strengths.

2.4. Electrochemical Properties

Reduction potentials for PIIG-NDI(OD), PIIG-PDI(EH), and PIIG-PDI(OD) were measured by cyclic voltammetry (CV) using ferrocene as the internal standard. Cyclic voltammograms of the polymers as thin films are shown in Figure S7 (Supporting Information), and electrochemical data are summarized in Table 1. HOMO and LUMO energies can be estimated based on these potentials and the optical bandgaps.[16] Based on half reductive potential, the LUMO energy level of PIIG-NDI(OD) is –3.93 eV, slightly higher than those of PIIG-PDI(EH) (–4.02 eV) and PIIG-PDI(OD) (–3.99 eV), which is consistent with the DFT calculations (Figure 3). This indicates that PIIG-NDI(OD) based solar cells may generate higher open-circuit voltages (V_{OC}).

2.5. All-Polymer Solar Cells

To evaluate the novel polymers as non-fullerene acceptors for all-polymer solar cells, bulk heterojunction solar cells were fabricated with PTB7-Th:polymers (mass ratio, 1:1) blend films in an inverted device structure of indium tin oxide (ITO)/ZnO/blend film/MoO_3/Ag and the thickness of the blend films were measured to be 60 nm. PTB7-Th was chosen as the donor due to its complementary UV–vis absorption with the novel n-type polymers (Figure 2c). Measurements were carried out under simulated AM 1.5G illumination of 100 mW cm^{-2}, and current density–voltage (J–V) curves are shown in **Figure 4**a. The corresponding V_{OC}, J_{SC}, fill factors (FF), and power conversion efficiencies (PCE) are summarized in **Table 2**.

PTB7-Th:PIIG-NDI(OD) based solar cells afford a moderate efficiency of 1.67% with a V_{OC} of 0.829 V, J_{SC} of 5.06 mA cm^{-2},

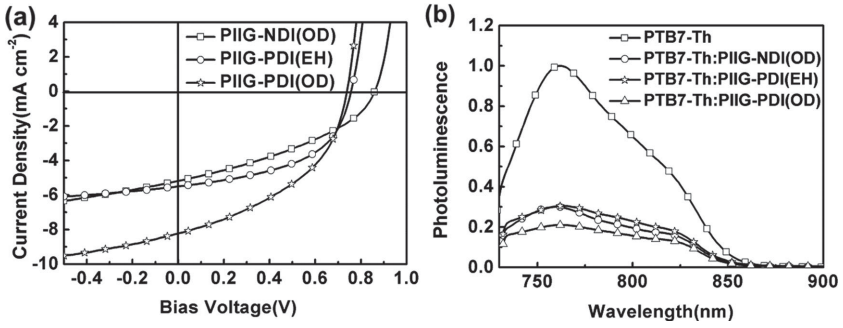

Figure 4. a) *J–V* curves of PTB7-Th:polymer (polymer, PIIG-NDI(OD), PIIG-PDI(EH), PIIG-PDI(OD)) based solar cells, and b) photoluminescence of PTB7-Th and PTB7-Th:polymer blend films.

and FF of 36.3%. The relatively small J_{SC} is consistent with its moderate photoluminescence quenching (70%). In comparison, the solar cells of PTB7-Th:PIIG-PDI(EH) blend films afford a PCE of 2.21% with a V_{OC} = 0.748 V, J_{SC} = 5.88 mA cm^{-2}, and FF = 50.2%, which is smaller than that of PTB7-Th:PIIG-PDI(OD) based solar cells (2.68%) with a V_{OC} = 0.738 V, J_{SC} = 8.22 mA cm^{-2}, and FF = 44.2%. Note this is the highest efficiency for all-polymer solar cells with A–A polymers as acceptors. The V_{OC} of both PIIG-PDI based solar cells is lower than those of PIIG-NDI(OD) based solar cells, attributed to the lower LUMO energy levels of PIIG-PDI polymers than that of PIIG-NDI(OD). This is because the smaller $HOMO_{PTB7\text{-}Th}$–$LUMO_{PIIG\text{-}PDI}$ offset generated lower V_{OC}. At the same time, J_{SC} of both PIIG-PDI based solar cells is higher than that of PIIG-NDI(OD), accordant with their stronger absorption in UV–vis spectra.

2.6. All-Polymer PDs

All-polymer PDs were fabricated with a thicker blend film (100 nm) of PTB7-Th:polymer (mass ratio, 1:1) in an inverted device structure of ITO/ZnO/blend/MoO_3/Ag. The inverted structure has advantages for integration with CMOS technology and avoiding the usage of moisture sensitive cathodes such as calcium or samarium generally used for the best fullerene based OPDs. **Figure 5**a shows the *J–V* characteristics of PTB7-Th: polymers based PDs in the dark and under illumination. The corresponding data are summarized in **Table 3**. At –0.2 V, the dark current densities (J_d) of PTB7-Th:PIIG-NDI(OD)-based PD is 2.8×10^{-7} A cm^{-2}. Replacing the moiety NDI(OD) with PDI(OD), the J_d of PTB7-Th:PIIG-PDI(OD) based PDs decreased to 1.2×10^{-7}. Furthermore, substitution of OD with EH alkyl chains, the J_d of PTB7-Th:PIIG-PDI(EH) based PDs decreased to 7.5×10^{-8} A cm^{-2}, substantially lower than that of PTB7-Th:PIIG-NDI(OD)-based PD. It is obvious that tuning the polymeric structures through changing the building blocks and alkyl chains can decrease the dark current of PDs. Significantly, the dark current of PTB7-Th:PIIG-PDI(EH) based PDs is comparable to the fullerene based OPDs.[2h,17] It should be noted that this low dark current was achieved without the use of hole or electron blocking layers.

Under AM 1.5G illumination, the photocurrent densities (J_{ph}) of PTB7-Th:PIIG-PDI(EH), PTB7-Th:PIIG-PDI(OD) based PDs are 4.14×10^{-3} and 6.09×10^{-3} A cm^{-2}, higher than that of PTB7-Th:PIIG-NDI(OD) based PDs (3.67×10^{-3} A cm^{-2}) (Table 3), in accordance with the current densities of OPVs. As results, the on/off ratio of J_d at –0.2 V for PIIG-PDI(EH)-based PDs is 5.5×10^5, several times higher than that of PIIG-NDI(OD)-based PDs (1.2×10^5) (Table 3). As shown in Figure 5d, the photoresponse of all three polymers-based devices cover the range from 350 to 800 nm, reaching the near-infrared edge. Furthermore, the EQEs for all three PDs systematically increased by increasing the reverse bias up to –1 V as shown in Figure S10 (Supporting Information), and typical curves of PTB7-Th:PIIG-PDI(EH) based PDs are shown in Figure 5b. Figure 5c showed the EQE characteristics of these three OPDs under negative bias of –1 V. For PTB7-Th: PIIG-NDI(OD)-based PDs, the EQE curves became extremely rough at –1 V, which means that the PDs started to be unstable. However, the EQE for PTB7-Th:PIIG-PDI(EH) and PTB7-Th:PIIG-PDI(OD)-based PDs demonstrated smooth curves and reached over 20% at –1 V. This showed that tuning the polymeric structures through changing building blocks from NDI to PDI can dramatically increase both EQE and the stability of the all-polymer PDs.

We also calculated the responsivity from the measured EQE with equation

$$R = EQE/h\nu \quad (1)$$

where $h\nu$ is the energy of the incident photon in eV. As shown in Figure S11 (Supporting Information), the responsivities for all three PDs continuously increased by increasing the reverse bias up to –1 V. Figure 5d shows calculated responsivities for PIIG-NDI(OD), PIIG-PDI(EH), PIIG-PDI(OD)-based all polymer PDs at –1.0 eV. It is not surprising that the responsivity of PIIG-NDI(OD)-based all-polymer PDs demonstrated a rough curve. The highest responsivity of PIIG-PDI(OD) and PIIG-PDI(EH)-based all-polymer PDs reached 0.12 A W^{-1}. This responsivity over the visible range is comparable to inorganic photodiodes and the fullerene based OPDs.[18]

To calculate the detectivity (D^*) of PDs, we used the equation

$$D^* = R/(2qJ_d)^{1/2} \quad (2)$$

Table 2. Photovoltaic performances of PTB7-Th based solar cells. The average values are from over ten devices.

Polymers	V_{OC} [V]	J_{SC} [mA cm^{-2}]	FF [%]	$PCE_{average}$ [%]	PCE_{max} [%]	μ_h [cm^2 V^{-1} s^{-1}]	μ_e [cm^2 V^{-1} s^{-1}]
PIIG-NDI(OD)	0.82 ± 0.01	5.06 ± 0.05	36.3 ± 0.3	1.68 ± 0.02	1.70	9.18×10^{-5}	4.56×10^{-7}
PIIG-PDI(EH)	0.73 ± 0.02	5.88 ± 0.03	50.2 ± 0.2	2.20 ± 0.01	2.21	1.83×10^{-4}	2.06×10^{-6}
PIIG-PDI(OD)	0.72 ± 0.02	8.22 ± 0.03	44.2 ± 0.2	2.65 ± 0.03	2.68	1.70×10^{-4}	5.90×10^{-5}

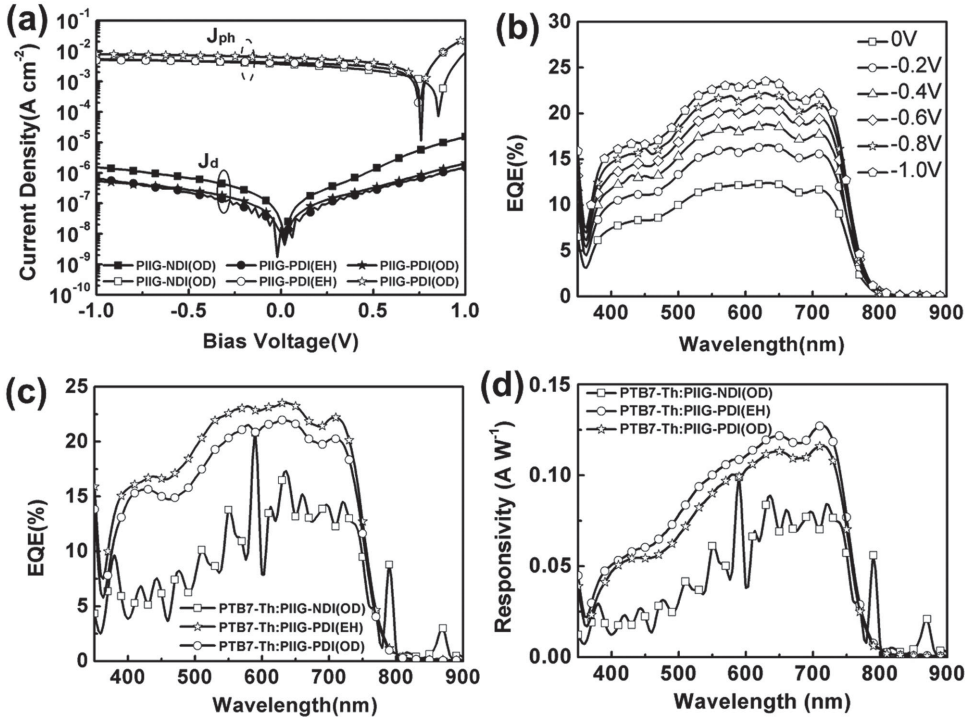

Figure 5. a) Current density–voltage (*J–V*) characteristics of PDs measured in the dark and under AM 1.5G (100 mW cm^{-2}) illumination, and b) the external quantum efficiency of PTB7-Th:PIIG-PDI(EH) based PDs at different voltage, and c) the external quantum efficiency and d) responsivity of PDs at –1 V.

where q is the absolute charge of 1.6×10^{-19} C, J_d is the dark current density in A cm^{-2}. The detectivities of the all polymer PDs at –0.2 V were shown in **Figure 6**a. For PIIG-NDI(OD)-based devices, the J_d was 2.8×10^{-7} A cm^{-2} at –0.2 V in dark. As a result, the devices show moderate detectivities of over 10^{10} Jones from 350 to 750 nm. Replacing NDI with PDI moiety, the PIIG-PDI(OD)-based devices exhibit enhanced detectivities of over 10^{11} Jones from 350 to 750 nm. Furthermore, tuning the structure through changing the alkyl chains, the detectivities of PIIG-PDI(EH)-based devices were further improved due to their low J_d (7.5×10^{-8} A cm^{-2}), resulting in a maximum detectivity of 0.6×10^{12} Jones, which is comparable to the performance of inorganic PDs and the fullerene based OPDs.[2j] These results demonstrated that tuning the polymeric structures with building blocks and alkyl chains can systematically improve the detectivity of the all-polymer PDs.

To determine these important parameters, low frequency noise current analysis was investigated. Figure 6b shows the measured noise current for the three polymers PDs at –1 V. It can be clearly observed that the noise current of the devices decreased with increasing modulation frequency. The PIIG-NDI(OD)-based devices exhibit moderate noise current close to 1×10^{-8} A Hz$^{-1/2}$ at a modulation frequency of 100 Hz under –1 V bias. In contrast, PIIG-PDI(OD)-based devices demonstrated much smaller noise current of 4×10^{-10} A Hz$^{-1/2}$ at the same frequency. Furthermore, noise current of PIIG-PDI(EH)-based devices continuously decreased to 1×10^{-10} A Hz$^{-1/2}$. The low noise currents presented in PIIG-PDI-based devices are favorable for small noise equivalent power (NEP) – the minimum input optical power that a detector can distinguish from noise. Using the equation

$$NEP = i_n / R \tag{3}$$

(i_n is the noise current in A, and R is the responsivity in A W^{-1}),[19] the NEP of the PIIG-PDI(OD) and PIIG-PDI(EH) detectors were calculated to be 3.9×10^{-9} and 1.5×10^{-9} W at 700 nm (–1 V, 100 Hz), respectively. This indicates that the PIIG-PDI(OD)-based PDs should be able to detect light intensity as low as 56 nW cm^{-2} at 700 nm (the area of devices, 0.07 cm^2), and PIIG-PDI(EH)-based PDs can detect light intensity as low as 21 nW cm^{-2} at 700 nm. In contrast, the PIIG-NDI(OD)-based detectors are not able to function at –1 V.

Table 3. The dark current J_d and photocurrent J_{ph} of polymer PDs with different electron donors.

Electron acceptor	J_d (–0.2 V) [A cm^{-2}]	J_d (–1 V) [A cm^{-2}]	J_{ph} (0 V) [A cm^{-2}]	I_{on}/I_{off} (–0.2 V)
PIIG-NDI(OD)	2.8×10^{-7}	1.55×10^{-6}	3.67×10^{-3}	1.2×10^{5}
PIIG-PDI(EH)	7.5×10^{-8}	6.77×10^{-7}	4.14×10^{-3}	5.5×10^{5}
PIIG-PDI(OD)	1.2×10^{-7}	5.45×10^{-7}	6.09×10^{-3}	5.2×10^{5}

2.7. Photoluminescence and Space-Charge-Limited Current

Exciton split is a critical step for OPVs and OPDs. To understand the exciton quenching of the blend films, photoluminscence (PL) spectra of PTB7-Th and the blend films were investigated

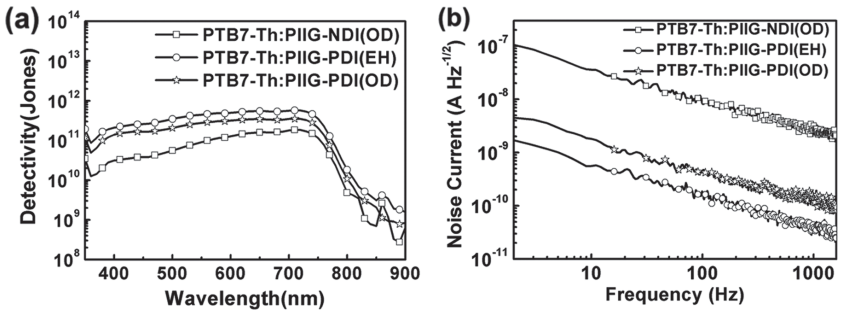

Figure 6. a) The detectivity of PDs at –0.2 V, and b) noise current of PDs measured at different frequencies.

as shown in Figure 4b. PTB7-Th demonstrated a broad peak in the range of 700–850 nm, while the blend films of PTB7-Th:polymers = 1:1 show evidence of quenched PL intensities, indicative of either energy or charge transfer processes. This suggested that the novel three n-type polymers are suitable for being electron acceptors for photovoltaics and PDs. Based on the PL quenching at the peak (761 nm), PTB7-Th:PIIG-PDI(OD) blend exhibits the most efficient quenching (80%), which suggesting that the PTB7-Th:PIIG-PDI(OD) blend can split the excitons most efficiently and potentially generate the highest photocurrent density. This is consistent with the highest J_{SC} and J_{ph} for PTB7-Th:PIIG-PDI(OD) based photovoltaics and PDs, respectively.

The space-charge-limited current (SCLC) method was employed to estimate the electron and hole transport mobilities of the blend films. Both estimated electron and hole mobilities are summarized in Table 2 and the typical $J^{1/2}$–V curve is shown in Figure S8 (Supporting Information). The PTB7-Th: PIIG-NDI (OD) blend film exhibits an unbalanced electron (9.18×10^{-5} cm^2 V^{-1} s^{-1}) and hole (4.56×10^{-7} cm^2 V^{-1} s^{-1}) mobilities, while PTB7-Th:PIIG-PDI(EH) blend film possesses faster electron (1.83×10^{-4} cm^2 V^{-1} s^{-1}) and hole (2.06×10^{-6} cm^2 V^{-1} s^{-1}) mobilities. Furthermore, PTB7-Th:PIIG-PDI(OD) blend film demonstrated the most balance electron (1.70×10^{-4} cm^2 V^{-1} s^{-1}) and hole (5.90×10^{-5} cm^2 V^{-1} s^{-1}) mobilities, indicating that this blend film collects charges most efficiently. This is accordant with the highest J_{SC} and J_{ph} of the PTB7-Th:PIIG-PDI(OD) based photovoltaics and PDs. Furthermore, thin film transistors (TFTs) were also fabricated for the polymers films without annealing. As shown in Figure S9 (Supporting Information), the PIIG-PDI(EH) and PIIG-PDI(OD) showed electron mobilities of 9.1×10^{-7} and 1.7×10^{-5} cm^2 V^{-1} s^{-1}, respectively. Furthermore, the PIIG-NDI(OD) based TFT devices is not active under the same condition. This observation is consistent with the trend of SCLC electron mobilities.

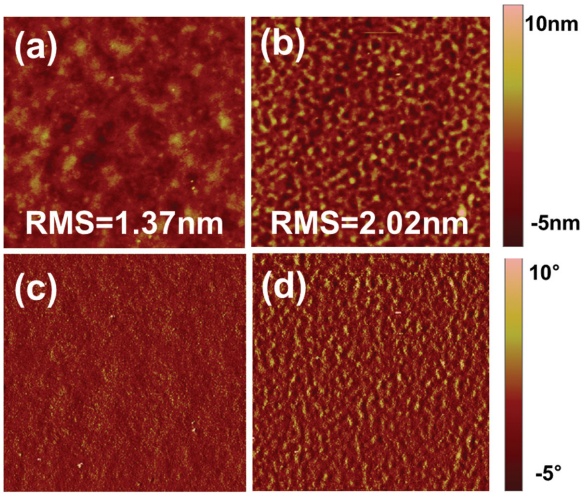

Figure 7. Tapping mode AFM topographic and phase images of a,c) PTB7-Th:PIIG-PDI(EH) and b,d) PTB7-Th:PIIG-PDI(OD).

2.8. Morphology Characterization

The optimal morphology of active layer, especially the domain size, is critically important for the performance of OPVs and OPDs. It is believed that polymer side chains can impact the solubility and miscibility with other polymers. The film morphology of the blend films should also be influenced by the side chains. Tapping-mode atomic force microscope (AFM) was employed to investigate the morphology of PTB7-Th:PIIG-PDI(EH) and PTH7-Th:PIIG-PDI(OD) blend films to understand the effect of alkyl chains. As shown in **Figure 7**a,b, the PTB7-Th:PIIG-PDI(EH) blend films demonstrated a smoother morphology with a root mean square roughness (RMS) of 1.37 nm than PTB7-Th:PIIG-PDI(OD) (RMS = 2.02 nm). The smoother surfaces could avoid the penetration of the top electrode into the active layer and afford a better contact with the top electrode, which may contribute for the reduction of J_d.[20] At the same time, it is clearly observed that PTB7-Th:PIIG-PDI(EH) blend film exhibits the formation of large and uncontinuous grains, which is usually not ideal for exciton separation and charge transport, as evident by low J_{SC} in OPVs and J_{ph} in OPDs. In contrast, the surface morphology of PTB7-Th:PIIG-PDI(OD) blend film shows much smaller domains with the bicontinuous interpenetrating networks, which is ideal for high photoresponse. Figure 7c,d showed the phase images of PTB7-Th:PIIG-PDI(EH) and PTB7-Th:PIIG-PDI(OD) blend films. Clearly, PTB7-Th:PIIG-PDI(OD) blend film showed a rougher but continuous interpenetrating domains, consistent with the topographic images.

3. Conclusion

In summary, three A–A conjugated polymers were synthesized and characterized. Through tuning the polymeric structure by changing the building blocks and alkyl chains, the photophysical properties of the copolymers and blend film morphologies were systematic optimized to afford high performance all-polymer solar cells and PDs. The efficiency of PTB7:PIIG-PDI(OD) based solar cells reaches 2.68%, which is one of the highest for A–A conjugated polymers systems. Furthermore, the first all-polymer PDs were obtained based on the novel n-type conjugated polymers. The responsivity is 0.12 A W^{-1} and the detectivity reaches 10^{12} Jones, which are among those of the

fullerene based OPDs and inorganic PDs. This contribution sheds light on the relationship between the polymeric structures and high performance all-polymer photoresponse devices.

4. Experimental Section

Materials: All chemicals were purchased from Energy Chemical, and used without further purification. Solvents for chemical synthesis were purified by distillation. Chemical reactions were carried out under a nitrogen atmosphere. The following compounds were synthesized according to the reported procedures: 6,6′-(*N*,*N*′-2-octyldodecyl)-pinacoldiboronisoindigo,[21,22] 2Br-NDI (OD),[23,24] 2Br-PDI (EH and OD).[25]

PIIG-NDI(OD): In a Schlenk tube (25 mL), 6,6′-(*N*,*N*′-2-octyldodecyl)-pinacoldiboronisoindigo (0.102 mmol), 2Br-NDI (0.102 mmol), K_3PO_4 (0.51 mmol), tetrabutylammonium chloride (50 mg) were dissolved in a mixed solvent of toluene (7 mL) and deionized (DI) water (1.5 mL). The mixture was bubbled with nitrogen for 15 min at room temperature. Then, Pd_2 (dba)$_3$ (1.4 mg, 1.5 μmol) and tri-o-tolylphosphine (1.9 mg, 6.1 μmol) were added to the reaction mixture and stirred at 100 °C for 2 d. Afterward, phenylboronic acid (40.8 mg, 0.2 mmol) was added. After the reaction mixture was stirred at 100 °C for 4 h, bromobenzene (62.8 mg, 0.4 mmol) was added and the reaction mixture was stirred for another 4 h to complete the end-capping procedure. The whole mixture was cooled to room temperature and dropped into CH_3OH (300 mL). After filtration, the crude product was dried in vacuum, and subjected to Soxhlet extraction with a sequence of acetone, hexane, tetrahydrofuran (THF), and $CHCl_3$. Finally, the $CHCl_3$ fraction was concentrated, reprecipitated into CH_3OH (300 mL), and filtered off through filter paper. The polymers were recovered as a black purple solid (116.3 mg, yield: 69%) M_n = 16184 kDa, M_w = 32554 kDa, *PDI* = 2.01.

^{1}H NMR (400 MHz, $CDCl_3$) δ (ppm) 9.56–9.35 (br, 2H), 8.79–8.69 (br, 2H), 7.18–7.01 (br, 2H), 6.91–6.76 (br, 2H), 4.44–3.44 (br, 8H), 2.19–1.85 (br, 4H), 1.60–1.05 (br, 128H), 0.95–0.75 (br, 24H). Anal. calcd. for $C_{110}H_{172}N_4O_6$: C, 80.14; H, 10.64; N, 3.40; found: C, 79.20; H, 10.18; N, 3.32.

PIIG-PDI: In a Schlenk tube (25 mL), diborate-isoindigo (0.10 mmol), dibromo-perylene diimide (0.10 mmol), K_3PO_4 (108.5 mg, 0.51 mmol), and tetrabutylammonium chloride (50 mg) were dissolved in a mixed solvent of toluene (7 mL) and deionized water (1.5 mL). The mixture was bubbled for 15 min with nitrogen at room temperature. Then, $Pd(PPh_3)_4$ (7 mg, 0.006 mmol) was added to the reaction mixture and stirred at 100 °C for 2 d. Afterward, phenylboronic acid (40.8 mg, 0.2 mmol) was added. After the reaction mixture was stirred at 100 °C for 4 h, bromobenzene (62.8 mg, 0.4 mmol) was added and the reaction mixture was stirred for another 4 h to complete the end-capping procedure. The whole mixture was cooled to room temperature and dropped into CH_3OH (300 mL). After filtration, the crude product was dried in vacuum, and subjected to Soxhlet extraction with a sequence of acetone, hexane, THF, and $CHCl_3$. Finally, the $CHCl_3$ fraction was concentrated, reprecipitated into CH_3OH (300 mL), and filtered off through filter paper. The polymer was recovered as a black purple solid.

PIIG-PDI(EH): Yield: 61%. M_n = 26944 kDa, M_w = 71154 kDa, *PDI* = 2.64. ^{1}H NMR (400 MHz, $CDCl_3$) δ (ppm) 9.65–9.30 (br, 2H), 8.85–8.55 (br, 2H), 8.43–8.21 (br, 2H), 8.19–7.98 (br, 2H), 7.50–7.30 (br, 2H), 7.09–6.82 (br, 2H), 4.50–3.14 (br, 8H), 2.13–1.81 (br, 4H), 1.80–0.89 (br, 80H), 0.87–0.67 (br, 24H). Anal. calcd. for $C_{96}H_{128}N_4O_6$: C, 80.29; H, 9.12; N, 3.90; found: C, 80.42; H, 9.02; N, 3.82.

PIIG-PDI(OD): Yield: 76%. M_n = 27637 kDa, M_w = 64620 kDa, *PDI* = 2.34. ^{1}H NMR (400 MHz, $CDCl_3$) δ (ppm) 9.65–9.30 (br, 2H), 8.85–8.55 (br, 2H), 8.43–8.21 (br, 2H), 8.19–7.98 (br, 2H), 7.50–7.30 (br, 2H), 7.09–6.82 (br, 2H), 4.50–3.14 (br, 8H), 2.13–1.81 (br, 4H), 1.80–0.89 (br, 128H), 0.87–0.67 (br, 24H). Anal. calcd. for $C_{20}H_{176}N_4O_6$: C, 80.29; H, 9.12; N, 3.90; found:C, 80.44; H, 9.88; N, 3.20.

Characterizations: The ^{1}H nuclear magnetic resonance (NMR) spectra were measured on a Bruker AVANCE 400 MHz NMR spectrometer using deuterated chloroform as the solvent. Tetramethylsilane was used as an internal reference for the NMR analysis. Elemental analysis was performed on a FLASH EA 1112 Elemental Analyzer. The electrochemical CV was carried out on a CHI600E electrochemical workstation in a solution of tetrabutylammonium hexafluorophosphate (Bu_4NPF_6) in dry acetonitrile as the supporting electrolyte with a scan rate of 50 mV s^{-1}. A Pt wire, glassy carbon disks, and Ag/AgCl were used as the counter, working electrode, and reference electrodes, respectively. A ferrocene/ferrocenium redox couple was used as an external standard. The potential was located at 0.5 eV, which was assumed to have an absolute energy lever of –4.44 eV to vacuum (LUMO = $-E_{red}$ – 4.44, HOMO = LUMO – E_g). UV–vis absorption spectra were carried out using a Cary 60 UV–vis Spectrophotometer at room temperature. All the film samples were spin coated on glass substrates. GPC analysis was conducted on a PL-GPC 220 system with polystyrene as a standard and 1,2,4-trichlorobenzene as eluent at 150 °C. TGA measurements were carried out using a Shimadzu thermogravimetric analyzer (model DTG-60) under a continuous nitrogen flow at a heating rate of 10 °C min^{-1}. DSC measurements were measured using a TA Instruments differential scanning calorimeter (Q2000) under nitrogen at a heating rate of 10 °C min^{-1}. AFM measurements were performed by using a Scanning Probe Microscope-Dimension 3100 in a tapping mode with all film samples spin-coated on ITO/ZnO substrates.

Fabrication and Characterization of Organic Thin Film Transistor (OTFT): Thin semiconductor films were deposited by spin-coating of a 6 mg mL^{-1} polymer solution in chloroform under ambient conditions onto hexamethyldisilazane (HMDS)-treated p-doped Si (001) wafers with a 300 nm thermally grown SiO_2 dielectric layer. The capacitance of the 300 nm SiO_2 gate insulator was 10 nF cm^{-2}. Prior to substrate treatment with HMDS, the wafers were solvent cleaned by sonicating (in two beakers, sequentially, for 15 min each) in EtOH and were then dried with a filtered stream of N_2, followed by 5 min plasma cleaning in a Harrick PDC-32G Plasma Cleaner/Sterilizer. After semiconductor deposition, the films were moved to the chamber. Top-contact OTFTs were fabricated by vapor deposition of gold electrodes (≈10^{-7} Torr, 0.2 Å s^{-1}, ≈50 nm thick) onto the semiconductor thin films through a shadow mask to obtain devices with channel widths and lengths of 5000 and 100 μm, respectively.

Fabrication and Characterization of OPV: The inverted device structure was ITO/ZnO/active layer/MoO_3/Ag. The ITO glass was cleaned sequentially in ultrasonic baths with DI water, acetone, and isopropanol for 30 min at each step. Then the ITO substrate was dried at 80 °C in an oven for 1 h and treated in an ultraviolet-ozone chamber for 30 min. The ZnO precursor solution prepared from 0.5 M zinc acetate dehydrate in 0.5 M monoethanolamine and 2-methoxyethanol was spin-coated onto the ITO glass at 4500 rpm for 40 s, annealed at 200 °C on a hot plate in air for 30 min. Subsequently, the substrate was transferred to the nitrogen-filled glove box, followed by the spin-coating of the active layer. Active layer (e.g., PTB7-Th:PIIG-NDI(OD) blend (1:1.5 w/w)) solution in chloroform was spin-coated at 3500 rpm for 30 s. The thickness of the active layer was about 60 nm. After dried under N_2 for 2 h, the thin films were transferred into a vacuum chamber of a thermal evaporator inside the glove box. MoO_3 (10 nm) and Ag (100 nm) were deposited sequentially by thermal evaporation under 10^{-5} Pa. The photoactive layer area of the device was 0.04 cm^2.

All *J*–*V* characterizations were performed under AM 1.5G using a Newport solar simulator (100 mW cm^{-2}).

Fabrication and Characterization of OPD: The inverted device structure was ITO/ZnO/active layer/MoO_3/Ag. The ITO glass was cleaned sequentially in ultrasonic baths with DI water, acetone, and isopropanol for 30 min at each step. Then the ITO substrate was dried at 80 °C in an oven for 1 h and treated in an ultraviolet-ozone chamber for 30 min. The ZnO precursor solution was spin-coated onto the ITO glass at 4500 rpm for 40 s, annealed at 200 °C on a hot plate in air for 30 min. Subsequently, the substrate was transferred to the nitrogen-filled glove box, followed by the spin-coating of the active layer. Active layer (e.g., PTB7-Th:PIIG-NDI(OD) blend (1:1.5 w/w)) solution in chloroform was spin-coated at 900 rpm for 30 s. The thickness of the active layer

was about 100 nm. After dried under N_2 for 2 h, the substrates were transferred into a vacuum chamber of a thermal evaporator inside the glove box. MoO_3 (10 nm) and Ag (100 nm) were deposited sequentially by thermal evaporation under 10^{-5} Pa. The photoactive layer area of the device was 0.07 cm^2.

The *J–V* measurement of the devices under AM 1.5G solar simulator illumination (100 mV cm^{-2}) was performed on a computer-controlled Keithley 2400 Source Measure Unit under N_2. The *J–V* characteristics of the devices in dark were also measured by this instrument.

Space-Charge-Limited Current Mobility Measurement: Hole and electron mobilities of conjugated polymers were measured with the method of SCLC. Hole-only or electron-only diodes were fabricated using the architectures: ITO/PEDOT(Poly(3.4-ethylenedioxythiophene)): PSS (Poly(styrenesulfonate))/blend film/MoO_3/Al for holes and ITO/ZnO/ blend film/Ca/Al for electrons. The mobilities were obtained by taking current–voltage curves and fitting the results to a space-charge-limited form, where the SCLC were described by

$$J = 9\varepsilon_0\varepsilon_r\mu(V_{appl} - V_{bi})^2/8L^3 \quad (4)$$

Where ε_o was the permittivity of free space (8.85×10^{-12} F m^{-1}), ε_r was the relative permittivity of the material (assumed to be 3), μ was the hole mobility, V_{appl} was the applied voltage, V_{bi} was the built-in voltage (for hole-only diodes, V_{bi} was 0.2 V; for electron-only diodes, V_{bi} was 0 V),[26] and *L* was the thickness of the film. By linearly fitting $J^{1/2}$ with V_{appl}–V_{bi}, the mobilities were extracted from the slope and *L*

$$\mu_h = slope^2 \times 8L^3/9\varepsilon_0\varepsilon_r \quad (5)$$

Molecular Modeling: The electronic structure of the small molecule was performed on DFT calculations by Gaussian 09 software package[27] using B3LYP hybrid functional with basis set 6-31G(d).[28] All the alkyl chains were replaced with methyl chains. Vertical electronic excitation energies were computed using the TDDFT approach.[29]

External Quantum Efficiency: The EQE spectra of devices were measured with a Newport QE measurement kit by focusing a monochromatic beam of light onto the devices, and the light modulation frequency was set to 35 Hz.

Noise Current: A fast Fourier transform signal analyzer and a current preamplifier were used to record the noise signal at different frequency under –1 V bias.

Supporting Information

Supporting Information is available from the Wiley Online Library or from the author.

Acknowledgements

X.W. and L.L. contributed equally to this work. The authors thank the NSFC (51303180, 21574135, and 51373024), Beijing Natural Science Foundation (2162043), One Hundred Talents Program of Chinese Academy of Sciences, and University of Chinese Academy of Sciences for financial support. The results of DFT calculation described in this paper were obtained on the China Scientific Computing Grid (ScGrid). The authors thank Saina Yang at Institute of Chemistry Chinese Academy of Sciences for TGA and elemental analysis.

Received: April 8, 2016
Revised: June 1, 2016
Published online: July 1, 2016

[1] a) L. Dou, Y. Liu, Z. Hong, G. Li, Y. Yang, *Chem. Rev.* **2015**, *115*, 12633; b) Y.-J. Cheng, S.-H. Yang, C.-S. Hsu, *Chem. Rev.* **2009**, *109*, 5868; c) W. Li, K. H. Hendriks, M. M. Wienk, R. A. J. Janssen, *Acc. Chem. Res.* **2016**, *49*, 78; d) L. Ye, S. Zhang, L. Huo, M. Zhang, J. Hou, *Acc. Chem. Res.* **2014**, *47*, 1595; e) X. Guo, A. Facchetti, T. J. Marks, *Chem. Rev.* **2014**, *114*, 8943.

[2] a) G. Yu, K. Pakbaz, A. J. Heeger, *Appl. Phys. Lett.* **1994**, *64*, 3422; b) Y. Yao, Y. Liang, V. Shrotriya, S. Xiao, L. Yu, Y. Yang, *Adv. Mater.* **2007**, *19*, 3979; c) A. Armin, R. D. Jansen-van Vuuren, N. Kopidakis, P. L. Burn, P. Meredith, *Nat. Commun.* **2015**, *6*, 6343; d) J. D. Zimmerman, V. V. Diev, K. Hanson, R. R. Lunt, E. K. Yu, M. E. Thompson, S. R. Forrest, *Adv. Mater.* **2010**, *22*, 2780; e) F. Guo, B. Yang, Y. Yuan, Z. Xiao, Q. Dong, Y. Bi, J. Huang, *Nat. Nanotechnol.* **2012**, *7*, 798; f) X. Gong, M. Tong, Y. Xia, W. Cai, J. S. Moon, Y. Cao, G. Yu, C. L. Shieh, B. Nilsson, A. J. Heeger, *Science* **2009**, *325*, 1665; g) Z. Liu, K. Parvez, R. Li, R. Dong, X. Feng, K. Mullen, *Adv. Mater.* **2015**, *27*, 669; h) L. Li, F. Zhang, J. Wang, Q. An, Q. Sun, W. Wang, J. Zhang, F. Teng, *Sci. Rep.* **2015**, *5*, 9181; i) I. K. Kim, X. Li, M. Ullah, P. E. Shaw, R. Wawrzinek, E. B. Namdas, S. C. Lo, *Adv. Mater.* **2015**, *27*, 6390; j) J. Qi, X. Zhou, D. Yang, W. Qiao, D. Ma, Z. Y. Wang, *Adv. Funct. Mater.* **2014**, *24*, 7605.

[3] A. Facchetti, *Mater. Today* **2013**, *16*, 123.

[4] G. Yu, J. Gao, J. C. Hummelen, F. Wudl, A. J. Heeger, *Science* **1995**, *270*, 1789.

[5] J. Qi, Y. Gao, X. Zhou, D. Yang, W. Qiao, D. Ma, Z. Y. Wang, *Adv. Mater. Interfaces* **2015**, *2*, 1400475/1.

[6] a) G. Li, R. Zhu, Y. Yang, *Nat. Photonics* **2012**, *6*, 153; b) Z. He, B. Xiao, F. Liu, H. Wu, Y. Yang, S. Xiao, C. Wang, T. P. Russell, Y. Cao, *Nat. Photonics* **2015**, *9*, 174; c) X. Ouyang, R. Peng, L. Ai, X. Zhang, Z. Ge, *Nat. Photonics* **2015**, *9*, 520; d) Y. Liu, J. Zhao, Z. Li, C. Mu, W. Ma, H. Hu, K. Jiang, H. Lin, H. Ade, H. Yan, *Nat. Commun.* **2014**, *5*, 5293.

[7] a) M. Lenes, S. W. Shelton, A. B. Sieval, D. F. Kronholm, J. C. Hummelen, P. W. M. Blom, *Adv. Funct. Mater.* **2009**, *19*, 3002; b) R. B. Ross, C. M. Cardona, D. M. Guldi, S. G. Sankaranarayanan, M. O. Reese, N. Kopidakis, J. Peet, B. Walker, G. C. Bazan, E. Van Keuren, B. C. Holloway, M. Drees, *Nat. Mater.* **2009**, *8*, 208.

[8] a) H. Yan, Z. Chen, Y. Zheng, C. Newman, J. R. Quinn, F. Dotz, M. Kastler, A. Facchetti, *Nature* **2009**, *457*, 679; b) H. Huang, Z. Chen, R. Ponce Ortiz, C. Newman, H. Usta, S. Lou, J. Youn, Y. Y. Noh, K. J. Baeg, L. X. Chen, A. Facchetti, T. J. Marks, *J. Am. Chem. Soc.* **2012**, *134*, 10966.

[9] a) Y. J. Hwang, B. A. Courtright, A. S. Ferreira, S. H. Tolbert, S. A. Jenekhe, *Adv. Mater.* **2015**, *27*, 4578; b) Y. J. Hwang, T. Earmme, B. A. Courtright, F. N. Eberle, S. A. Jenekhe, *J. Am. Chem. Soc.* **2015**, *137*, 4424; c) E. Zhou, J. Cong, Q. Wei, K. Tajima, C. Yang, K. Hashimoto, *Angew. Chem. Int. Ed. Engl.* **2011**, *50*, 2799; d) H. Benten, T. Nishida, D. Mori, H. Xu, H. Ohkita, S. Ito, *Energy Environ. Sci.* **2016**, *9*, 135; e) Y. Geng, B. Xiao, S. Izawa, J. Huang, K. Tajima, Q. Zeng, E. Zhou, *J. Mater. Chem. A* **2015**, *3*, 22325; f) H. Lin, S. Chen, Z. Li, J. Y. L. Lai, G. Yang, T. McAfee, K. Jiang, Y. Li, Y. Liu, H. Hu, J. Zhao, W. Ma, H. Ade, H. Yan, *Adv. Mater.* **2015**, *27*, 7299; g) P. Cheng, L. Ye, X. Zhao, J. Hou, Y. Li, X. Zhan, *Energy Environ. Sci.* **2014**, *7*, 1351; h) W. Yu, D. Yang, X. Zhu, X. Wang, G. Tu, D. Fan, J. Zhang, C. Li, *ACS Appl. Mater. Interfaces* **2014**, *6*, 2350; i) W. Li, W. S. Roelofs, M. Turbiez, M. M. Wienk, R. A. Janssen, *Adv. Mater.* **2014**, *26*, 3304; j) M. Schubert, B. A. Collins, H. Mangold, I. A. Howard, W. Schindler, K. Vandewal, S. Roland, J. Behrends, F. Kraffert, R. Steyrleuthner, Z. Chen, K. Fostiropoulos, R. Bittl, A. Salleo, A. Facchetti, F. Laquai, H. W. Ade, D. Neher, *Adv. Funct. Mater.* **2014**, *24*, 4068; k) I. H. Jung, W.-Y. Lo, J. Jang, W. Chen, D. Zhao, E. S. Landry, L. Lu, D. V. Talapin, L. Yu, *Chem. Mater.* **2014**, *26*, 3450; l) A. Babel, S. A. Jenekhe, *J. Am. Chem. Soc.* **2003**, *125*, 13656; m) R. Stalder, J. Mei, J. Subbiah, C. Grand, L. A. Estrada, F. So, J. R. Reynolds, *Macromolecules* **2011**, *44*, 6303; n) Y. Zhou, T. Kurosawa, W. Ma, Y. Guo, L. Fang, K. Vandewal, Y. Diao, C. Wang, Q. Yan, J. Reinspach, J. Mei, A. L. Appleton, G. I. Koleilat, Y. Gao, S. C. Mannsfeld, A. Salleo,

H. Ade, D. Zhao, Z. Bao, *Adv. Mater.* **2014**, *26*, 3767; o) H. Huang, N. Zhou, R. P. Ortiz, Z. Chen, S. Loser, S. Zhang, X. Guo, J. Casado, J. T. López Navarrete, X. Yu, *Adv. Funct. Mater.* **2014**, *24*, 2782; p) X. Li, P. Sun, Y. Wang, H. Shan, J. Xu, C. You, Z.-X. Xu, Z.-K. Chen, *Polym. Chem.* **2016**, *7*, 2230; q) L. Gao, Z. G. Zhang, L. Xue, J. Min, J. Zhang, Z. Wei, Y. Li, *Adv. Mater.* **2016**, *28*, 1884.

[10] a) W. Jiang, Y. Li, Z. Wang, *Acc. Chem. Res.* **2014**, *47*, 3135; b) X. Zhan, A. Facchetti, S. Barlow, T. J. Marks, M. A. Ratner, M. R. Wasielewski, S. R. Marder, *Adv. Mater.* **2011**, *23*, 268.

[11] a) J. K. Lee, M. C. Gwinner, R. Berger, C. Newby, R. Zentel, R. H. Friend, H. Sirringhaus, C. K. Ober, *J. Am. Chem. Soc.* **2011**, *133*, 9949; b) M. C. Gwinner, T. J. K. Brenner, J.-K. Lee, C. Newby, C. K. Ober, C. R. McNeill, H. Sirringhaus, *J. Mater. Chem.* **2012**, *22*, 4436; c) X. Zhao, Y. Wen, L. Ren, L. Ma, Y. Liu, X. Zhan, *J. Polym. Sci., Part A: Polym. Chem.* **2012**, *50*, 4266; d) C.-W. Ge, C.-Y. Mei, J. Ling, J.-T. Wang, F.-G. Zhao, L. Liang, H.-J. Li, Y.-S. Xie, W.-S. Li, *J. Polym. Sci., Part A: Polym. Chem.* **2014**, *52*, 1200; e) J. L. Banal, J. Subbiah, H. Graham, J.-K. Lee, K. P. Ghiggino, W. W. H. Wong, *Polym. Chem.* **2013**, *4*, 1077.

[12] R. Zhao, C. Dou, Z. Xie, J. Liu, L. Wang, *Angew. Chem. Int. Ed. Engl.* **2016**, *55*, 5313.

[13] S. M. Sze, K. K. Ng, *Physics of Semiconductor Devices*, John Wiley & Sons, NJ, USA **2006**.

[14] J. A. Rogers, Z. Bao, K. Baldwin, A. Dodabalapur, B. Crone, V. R. Raju, V. Kuck, H. Katz, K. Amundson, J. Ewing, P. Drzaic, *Proc. Natl. Acad. Sci. USA* **2001**, *98*, 4835.

[15] H. Sirringhaus, T. Kawase, R. H. Friend, T. Shimoda, M. Inbasekaran, W. Wu, E. P. Woo, *Science* **2000**, *290*, 2123.

[16] H. Usta, C. Risko, Z. Wang, H. Huang, M. K. Deliomeroglu, A. Zhukhovitskiy, A. Facchetti, T. J. Marks, *J. Am. Chem. Soc.* **2009**, *131*, 5586.

[17] a) B. Yao, X. Zhou, X. Ye, J. Zhang, D. Yang, D. Ma, X. Wan, *Org. Electron.* **2015**, *26*, 305; b) G. Pace, A. Grimoldi, D. Natali, M. Sampietro, J. E. Coughlin, G. C. Bazan, M. Caironi, *Adv. Mater.* **2014**, *26*, 6773.

[18] X. Zhou, D. Yang, D. Ma, *Adv. Opt. Mater.* , **2015**, *3*, 1570.

[19] a) L. Dou, W.-H. Chang, Y. Yang, M. Yang Yang, J. You, Z. Hong, G. Li, *Nat. Commun.* **2014**, *5*, 5404; b) G. Konstantatos, I. Howard, A. Fischer, S. Hoogland, J. Clifford, E. Klem, L. Levina, E. H. Sargent, *Nature* **2006**, *442*, 180.

[20] L. Zhang, T. Yang, L. Shen, Y. Fang, L. Dang, N. Zhou, X. Guo, Z. Hong, Y. Yang, H. Wu, J. Huang, Y. Liang, *Adv. Mater.* **2015**, *27*, 6496.

[21] T. Lei, Y. Cao, Y. Fan, C.-J. Liu, S.-C. Yuan, J. Pei, *J. Am. Chem. Soc.* **2011**, *133*, 6099.

[22] G. Kim, A. R. Han, H. R. Lee, J. Lee, J. H. Oh, C. Yang, *Chem. Commun.* **2014**, *50*, 2180.

[23] R. Kim, P. S. K. Amegadze, I. Kang, H.-J. Yun, Y.-Y. Noh, S.-K. Kwon, Y.-H. Kim, *Adv. Funct. Mater.* **2013**, *23*, 5719.

[24] S. Vasimalla, S. P. Senanayak, M. Sharma, K. S. Narayan, P. K. Iyer, *Chem. Mater.* **2014**, *26*, 4030.

[25] Z. Mahmood, K. Xu, B. Küçüköz, X. Cui, J. Zhao, Z. Wang, A. Karatay, H. G. Yaglioglu, M. Hayvali, A. Elmali, *J. Org. Chem.* **2015**, *80*, 3036.

[26] J. Zhao, Y. Li, H. Lin, Y. Liu, K. Jiang, C. Mu, T. Ma, J. Y. Lin Lai, H. Hu, D. Yu, H. Yan, *Energy Environ. Sci.* **2015**, *8*, 520.

[27] Gaussian 09, Revision C.01, M. J. Frisch, G. W. Trucks, H. B. Schlegel, G. E. Scuseria, M. A. Robb, J. R. Cheeseman, G. Scalmani, V. Barone, B. Mennucci, G. A. Petersson, H. Nakatsuji, M. Caricato, X. Li, H. P. Hratchian, A. F. Izmaylov, J. Bloino, G. Zheng, J. L. Sonnenberg, M. Hada, M. Ehara, K. Toyota, R. Fukuda, J. Hasegawa, M. Ishida, T. Nakajima, Y. Honda, O. Kitao, H. Nakai, T. Vreven, J. A. Montgomery Jr., J. E. Peralta, F. Ogliaro, M. Bearpark, J. J. Heyd, E. Brothers, K. N. Kudin, V. N. Staroverov, T. Keith, R. Kobayashi, J. Normand, K. Raghavachari, A. Rendell, J. C. Burant, S. S. Iyengar, J. Tomasi, M. Cossi, N. Rega, J. M. Millam, M. Klene, J. E. Knox, J. B. Cross, V. Bakken, C. Adamo, J. Jaramillo, R. Gomperts, R. E. Stratmann, O. Yazyev, A. J. Austin, R. Cammi, C. Pomelli, J. W. Ochterski, R. L. Martin, K. Morokuma, V. G. Zakrzewski, G. A. Voth, P. Salvador, J. J. Dannenberg, S. Dapprich, A. D. Daniels, O. Farkas, J. B. Foresman, J. V. Ortiz, J. Cioslowski, D. J. Fox, *Gaussian, Inc.*, Wallingford CT, **2010**.

[28] A. D. Becke, *J. Chem. Phys.* **1993**, *98*, 1372.

[29] a) E. Runge, E. K. U. Gross, *Phys. Rev. Lett.* **1984**, *52*, 997; b) E. K. U. Gross, W. Kohn, *Advances in Quantum Chemistry* (Ed: L. Per-Olov), Vol. *21*, Academic Press, Santa Barbara, CA, USA, **1990**, p. 255; c) E. K. U. Gross, C. A. Ullrich, U. J. Gossmann, in *Density Functional Theory* (Eds: E. K. U. Gross, R. M. Dreizler), Springer US, Boston, MA **1995**, p. 149.